Chemical conversion of MoS2 thin films deposited by atomic layer deposition (ALD) into molybdenum nitride monitored by in situ reflectance measurements

J. Patouillard, R. Gassilloud, F. Mercier, A. Mantoux, R. Boichot, A. Crisci, M. Bernard, N. Gauthier, S. Cadot, C. Raynaud, et al.

Journal of Vacuum Science & Technology A

Chemical conversion of MoS_2 thin films deposited by Atomic Layer Deposition (ALD) into molybdenum nitride monitored by *in situ* reflectance measurements

J. Patouillard [1,2,3], R. Gassilloud [2], F. Mercier [1], A. Mantoux [1], R. Boichot [1], A. Crisci [1], M. Bernard [2], N. Gauthier [2], S. Cadot [2], C. Raynaud [2], F. Gianesello [3], E. Blanquet [1]

[1] Univ. Grenoble Alpes CNRS, Grenoble INP, SIMaP, 38000 Grenoble, France
[2] Univ. Grenoble Alpes, FR-38000 Grenoble, CEA, LETI, Minatec Campus, FR-38054 Grenoble Cedex 9, France. *E-mail: remy.gassilloud@cea.fr*
[3] STMicroelectronics, 850 rue Jean Monnet, F-38926 Crolles, France

Abstract

Two-dimensional (2D) metal nitrides are new emerging materials with potential applications in electronics, energy storage or conversion efficiency. In this paper, we report the synthesis of molybdenum nitride by nitriding molybdenum disulfide (MoS_2) via a 700 °C ammonia (NH_3) reactive heat treatment. A well-controlled uniform MoS_2 thin film was prepared by Atomic Layer Deposition (ALD). The progressive MoS_2 nitriding reaction has been demonstrated and monitored by *in situ* reflectance measurements. These results have been confirmed by Raman and X-Ray Photoelectron Spectrometry (XPS). This method paves the way to a new potential route to the synthesis of Mo nitride obtained from a well-controlled uniform 2D-MoS_2 thin film deposited by ALD.

I. Introduction

In 2004, Novoselov et *al.* [1] isolated graphene and demonstrated that materials with ultrathin thicknesses, also called two-dimensional (2D) materials can manifest different properties compared to their bulk counterparts. This finding opened the door to the emergence of new 2D nanomaterials such as metal oxides [2,3], transition metal dichalcogenides (TMDs) [4,5] or metal carbides and nitrides (MXenes) [6,7].

In recent years, metal nitrides have attracted attention due to their remarkable physical and chemical properties such as high electrical conductivities, catalytic properties, energy storage, and conversion efficiency. [8–12] However, even though chemical exfoliation methods

for preparing molybdenum nitrides nanosheets have been investigated and have led to the fabrication of dozen of nanometer thick films [13], to our knowledge, little amount of reports are focused on direct gas-phase synthesis [14], such as ALD, as done for MoS_2. In fact, the review of literature on MoN ALD literature shows that it is possible to deposit successfully MoN_x films but, despite a strong need, only a few studies have been reported. Various precursors and reagents of Mo have been studied, such as $MoCl_5$, which leads to quite good results in terms of resistivity but produces corrosive by-products [15] Other precursors $Mo(CO)_6$ has also been tested but one of the main concern with thermal ALD is the significant amount of oxygen in the films [16]. In the case of PEALD, the only report from Joo et *al.* [14] using $Mo(CO)_6$ and NH_3 indicates the formation of Cubic Mo_2N or MoCN. After annealing, crystalline Mo oxide is formed, confirming the poor stability of Mo nitride. That is why we are interested in an alternative route: starting from the more robust MoS_2 ALD process and the, apply a heat treatment under NH_3.

Among the transition metal disulfides MoS_2 is one of the most widely studied materials in recent years to synthetize molybdenum nitride due to its availability [17]. MoS_2 has a natural two-dimensional structure with the sandwich-like S-Mo-S layers serving as building blocks, where the atoms in the layer are linked by strong covalent bonds, while the layers are packed together by weak interlayer forces [18,19]. Its synthesis by Atomic Layer Deposition (ALD) methods is well-known in the literature allowing the deposition of large-scale and reproducible few MoS_2 monolayers. [20] Pioneering studies on the preparation of molybdenum nitrides by nitriding MoS_2 were initiated by Marchand et *al.* [21,22] by a direct reduction of sulfides in nitrides with ammonia. Recently, Sun et *al.* [13] and Cao et *al.* [23] have demonstrated the transformation of MoS_2 nanosheets exfoliated from bulk material into molybdenum nitride with ammonia and urea reactive heat treatments, respectively.

This work proposes to use *in situ* reflectance measurements to highlight the chemical conversion of a well-controlled uniform MoS_2 thin film deposited by Atomic Layer Deposition (ALD) into molybdenum nitride via an ammonia reactive heat treatment at 700 °C. Raman Spectroscopy, X-Ray Photoelectron Spectroscopy analysis are applied to characterize the samples and to support the *in situ* measurements.

II. Materials and Methods

MoS_2 samples were deposited by ALD on Si/SiO_2 (500 nm ± 20 nm) substrate at 90 °C using the process described in Cadot et *al.* [20] study. However, the annealing process was optimized and is achieved at 900 °C during 30 seconds at atmospheric pressure. This process has been transferred to an industrial ALD reactor in contrast Cadot et *al.* [20] where a custom-built CVD-ALD reactor is used. The MoS_2 preparation leads to the formation of well-controlled and uniform three monolayers MoS_2 thin film as shown in the TEM cross section in Figure 1 a). To determine the average MoS_2 thickness, we also performed X-Ray Reflectometry (XRR) measurements. The XRR pattern of a Si/SiO_2 (500 nm) sample is presented in Figure S1. After fitting, the resulting MoS_2 thickness is around 2.0 nm, which is consistent with a 3-4 monolayers MoS_2 thin film and the observation of the TEM-cross section. In addition, each Si/SiO_2/(500 nm)/MoS_2 samples were characterized by Raman spectroscopy before and after each heat treatment. A typical Raman spectrum of these samples before any heat treatment is presented in Figure 1 b). The peak at ≈ 520 cm^{-1} is due to the Si substrate, and is used as reference to adjust the position of the spectra. Two well-known pronounced E^1_{2g} and A_{1g} modes at ≈ 382.6 ± 0.2 cm^{-1} and ≈ 407.9 ± 0.1 cm^{-1} are attributed to MoS_2 [24,25] and also described in Figure 1 b). The E^1_{2g} mode corresponds to an in-plane vibration (perpendicular to c-axis) while A_{1g} is an out-of-plane vibration (along c-axis) [26].

a)

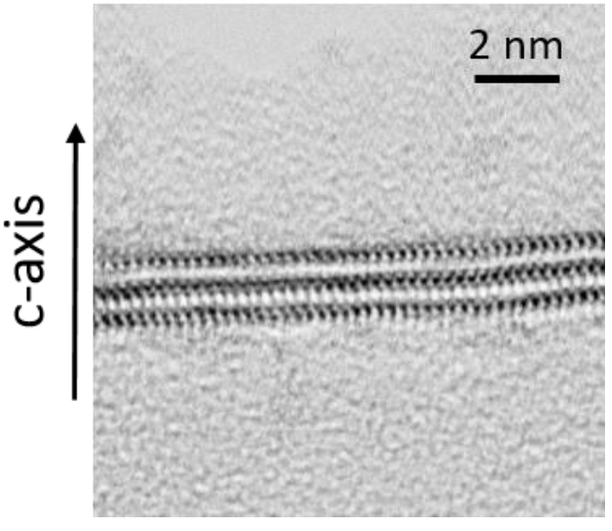

b)

Journal of Vacuum Science & Technology A

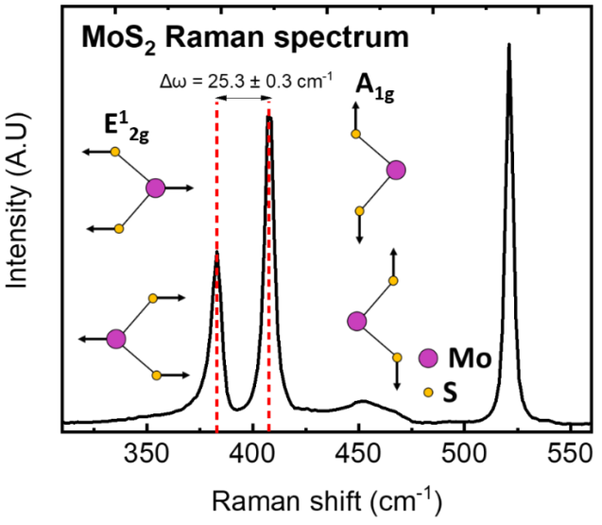

Figure 1: a) TEM cross-section of a Si/SiO_2 (500 nm)/MoS_2 sample. We observe three well-crystallized and uniform MoS_2 monolayers ; b) Typical Raman spectrum of a Si/SiO_2 (500 nm)/MoS_2 sample and schematic E^1_{2g} and A_{1g} active Raman modes of MoS_2

MoS_2 nitridation treatments were carried out in a home-made furnace at a temperature of 700 °C during 1 hour. Photos of the furnace and its components are shown in Figure 2. The furnace is equipped with a LayTec EpiTT system to monitor *in situ* reflectances with three different wavelengths at 405 nm, 633 nm and 949 nm labelled R405, R633 and R949, respectively. The reflectance is calculated from the ratio (value between 0 and 1) of the reflected luminous flux to the incident luminous flux. It is worth to notice that the *in situ* reflectance measurements system is equipped with a pyrometer directly pointing the sample surface with a detection range starting at 400 °C. The home-made furnace is equipped with a thermocouple with a temperature range adapted to lower temperatures. Hence, the samples have been removed around 80 °C for *ex situ* characterizations in order to prevent their oxidation.

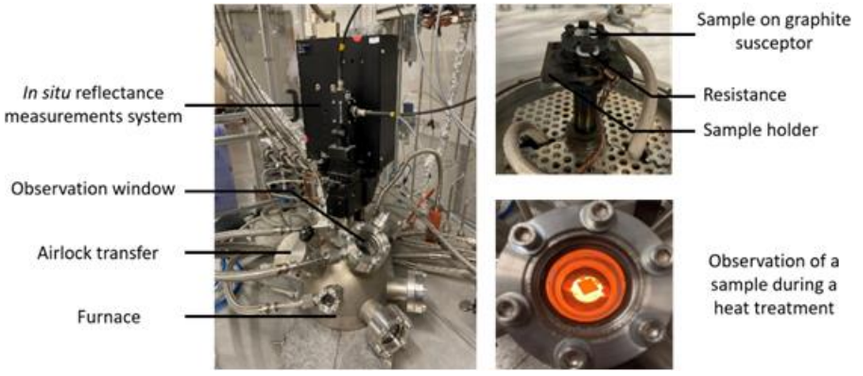

Figure 2: Description of the home-made furnace equipped with in situ reflectance measurements system, sample holder and observation of a sample during a heat treatment.

First, experiments were carried out under vacuum at a base pressure of 0.05 mbar. Subsequently, for NH_3 experiments, the flow rate of ammonia was set at 50 sccm and applied only during the temperature plateau. The NH_3 pressure varied at 0.5 mbar, 10 mbar, 30 mbar and 50 mbar using a throttle valve.

Raman spectra were collected in the backscattering geometry using a Renishaw In-Via spectrometer equipped with a Peltier cooled charge coupled device detector. The light was focused onto the sample surface using a x100 (0.85 numerical aperture) short working objective lens (0.27 mm). The resulting spot diameter was around 0.7 µm. A 532 nm wavelength laser diode was used as light source. The laser power was adjusted to not modify the material (1mW). Raman spectra experimental line shapes were fitted with Gaussian–Lorentzian components using the WiRE® software.

The XPS spectra were recorded with a PHI 5000 VersaProbe II spectrometer (Physical Electronics) using monochromatic Al K_α radiation (1486.6 eV) and with an overall energy resolution of 0.6 eV (with silver as reference). The analysis angle was set at 45°. Data treatment of the measured spectra were analysed using CasaXPS® software. For spectral calibration, C*1s* core peak from adventitious carbon was considered with binding energy at 284.8 eV. A non- linear Shirley-type background was processed for peak fitting and the deconvolution of the peaks was obtained using 30% Lorentzian and 70 % Gaussian line shapes.

III. Results

A. Experiments under vacuum

A first set of *in situ* reflectance experiments at 700 °C and 1000°C have been were performed to determine the behaviour of MoS_2 under vacuum in the furnace. These are considered at the reference tests, as no reactive gases are involved. These results are visible in Figure 3 a) at 1000°C and Figure 3 b) at 700°C. In this first set of experiments at 0.05 mbar, we varied the temperature imposing plateaus at 500°, 700°C and 1000°C (the temperature profile is plotted in black in the bottom of each graph) to adjust and find the optimal process conditions for the treatment under NH_3. We recorded the color change of the sample surface during each experiment by following the purple wavelength at 405nm, the orange at 633 nm, and the far red at 949nm.

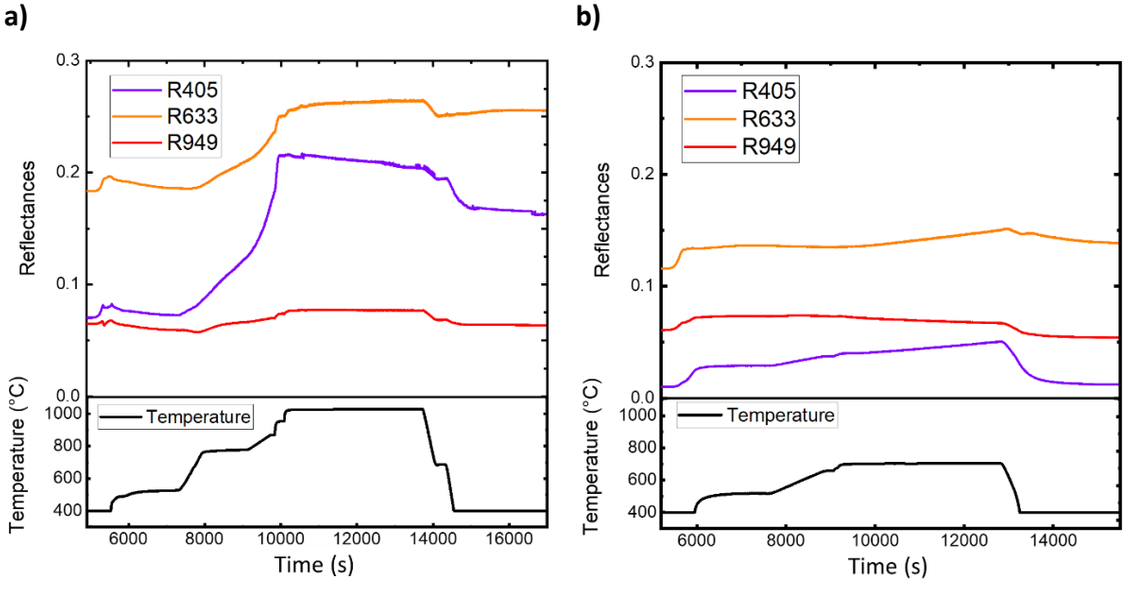

Figure 3: Under vacuum experiments, temperature profiles ramping-up to a) 1000°C ; b) 700°C. The purple component is very sensible to color changes at the surface. Nearly not changes are visible at 700°C, which indicates that the temperature is not high enough to induce surface modifications.

For the 1000°C experiment (Figure 3 a)), we observe a drastic increase in R405 and R633 from around 500°C up to 1000°C while there is nearly no change in R949. During the 1000°C temperature plateau, R405, R633 and R949 remain almost constant, and then they slightly decrease at the end of the experiment. This result shows that the surface color has clearly changed during the experiment, and that at the end of the annealing procedure the final

surface state has change, at least in color, but probably also in composition. We also performed the same test on another sample, but at lower temperature as shown in Figure 3 b). Compared to the 1000°C case, the 700°C experiment shows nearly no change in the color components all along the anneal profile, indicating that 700°C is probably not high enough to induce a color change, and subsequent structural modification. Also, we see that the purple based sensor is more sensible to any change of the sample surface, therefore in the rest of this work, we focalize the results on the 405nm wavelength contribution.

To confirm the modifications of the MoS_2 film at 1000°C under vacuum, we achieved Raman analysis and X-ray photoelectron spectroscopy on the samples after each heat treatment. The Raman spectra are visible in Figure 4. The E^1_{2g} and A_{1g} MoS_2 Raman modes are highlighted in the inset. As for the reference MoS_2 Raman spectrum presented in Figure 1 a) (and, the sample annealed at 700°C shows the two E^1_{2g} and A_{1g} vibration, while at 1000°C both Raman mode vanished completely, which indicates a clear disappearance of the MoS_2 layer. It is well known that the E^1_{2g} and A_{1g} Raman positions of MoS_2, and more precisely, the separation distance between both modes ($\Delta\omega$) are sensitive to the number of layers. Here, the difference between both modes are not totally in agreement with a three monolayers MoS_2 thin film [27]. However, previous works addressing with the influence of MoS_2 layer number on the Raman spectrum are mostly focused on MoS_2 exfoliated from bulk material [27–31]. It has been demonstrated for MoS_2 that growth methods and deposition conditions can lead to significant variations in Raman peaks positions [32,33].

Recently, Tuschel [34] has reported a $\Delta\omega$ value of 25 cm^{-1} for a three layers MoS_2 thin film prepared by chemical vapor deposition on silicon substrates, which is in good agreement with the values reported in this study. Raman Full Width at Half Maximum (FWHM) and positions of these modes before and after the 700 °C heat treatment are presented in Table 1. We observe that the FWHM and position of E^1_{2g} mode are not affected by the 700 °C vacuum heat treatment. In contrast, for A_{1g} mode, an increase in FWHM value and a redshift is observed after the heat treatment. It suggests a slight degradation of the MoS_2 layers after the heat treatment, yet the layers remain relatively well-crystallized.

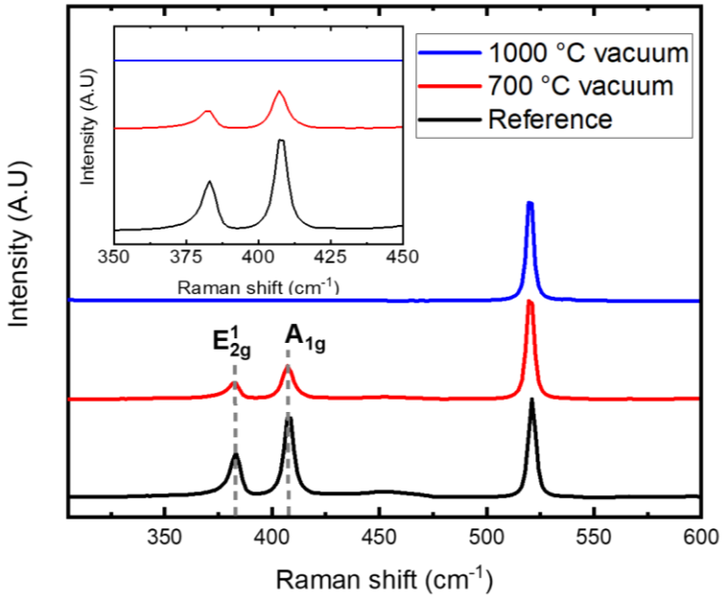

Figure 4: Raman spectra of a reference Si/SiO_2 (500 nm)/MoS_2 sample (black) before heat treatment and after 700°C (red) and 1000°C (blue) vacuum heat treatment. The inset focused on E^1_{2g} and A_{1g} MoS_2 Raman modes.

		Reference	700 °C vacuum
E^1_{2g}	Position (cm^{-1})	382.6 ± 0.2	382.3 ± 0.1
	FWHM (cm^{-1})	5.1 ± 0.3	4.7 ± 0.2
A_{1g}	Position (cm^{-1})	407.9 ± 0.1	407.3 ± 0.1
	FWHM (cm^{-1})	5.1 ± 0.2	5.6 ± 0.1
	Δω (cm^{-1})	25.3 ± 0.3	25.0 ± 0.2

Table 1: Positions and FWHM values of E^1_{2g} and A_{1g} Raman modes for the Si/SiO_2 (500 nm)/MoS_2 reference sample before and after 700 °C vacuum heat treatment.

These results presented above were confirmed by XPS characterizations. Binding energies positions and atomic concentrations of the MoS_2 reference sample, as well as the samples treated at 700 °C and 1000 °C are detailed in Table S1 of the Supplementary Information. High-resolution XPS spectra for Mo *3d* region are shown in Figure 5. For the MoS_2 reference sample and the treated sample after 700 °C heat treatment, the main part of the spectra is composed of two peaks at 229.8 eV and 232.8 eV attributed to spin-orbit doublets: Mo^{4+} $3d_{5/2}$ and Mo^{4+} $3d_{3/2}$, respectively. Their binding energies are assigned to MoS_2 environment and are in agreement with values found in literature [35–37]. The Mo $3d_{5/2}$ and Mo $3d_{3/2}$ peaks at 233.4 eV and 236.5 eV are attributed to Mo^{6+} state corresponding to a small amount of MoO_3 at the top surface [38,39]. We can also observed a slight peak at 227.0 eV which is attributed to S*2s*. Finally, and as expected, no contributions were observed in the Mo*3d* region for the 1000°C annealed sample. This suggests that the Mo element has been desorbed from the surface,

possibly in the form of a MoO_x volatile molecule, as a result of reaction wih residual oxygen. It is well known for the Mo-O system that Mo under pure O_2 is volatized in the form of MoO_3 gas above 700°C. This fact coupled with the relative long annealing time used during the experiment (i.e. a plateau of around 1h at 1000°C) can explain the absence of Mo at 1000°C and a reduction in the number of 2D plans at 700°C.

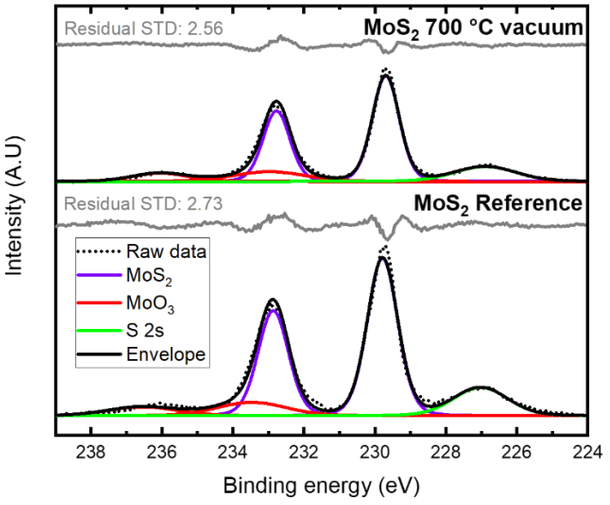

Figure 5: X-ray photoelectron spectroscopy (XPS) spectra of Mo 3d, for the MoS_2 reference sample (bottom) and the MoS_2 sample after 700 °C vacuum heat treatment (top).

B. MoS_2 nitridation treatments

After having optimized the process conditions under vacuum, a reactive heat treatment under NH_3 at a controlled pressure of 0.5 mbar and 50 mbar was applied to the MoS_2 samples. Figure 6 compare the *in situ* R405 reflectance of the 700 °C heat treatment at 0.5 mbar and 50 mbar. The NH_3 plateau is located between the vertical dash lines. A significant difference could be clearly observed between the heat treatment at 0.5 mbar and 50 mbar. As soon as the NH_3 valve is opened, a rapid increase in R405 followed by a plateau is observed for the heat treatment under 50 mbar while a progressive increase is observed for the 0.5 mbar treatment. In addition, the R405 reflectance value at the beginning and at the end of each ammonia treatment is different, contrary to those observed under vacuum at 700 °C (Figure 3 b).

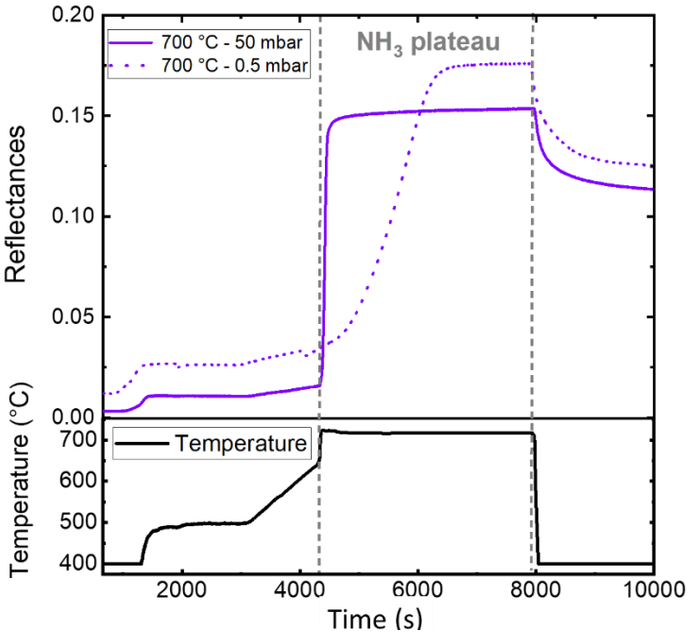

Figure 6: 700 °C NH_3 experiment with a regulated pressure of 50 mbar (solid line) and 0.5 mbar (dash line). The R405 component is very sensitive during the NH_3 experiment while it is almost constant during the vacuum experiment (except for the decrease in temperature).

The observed behavior indicates that the optical properties of the initial MoS_2 sample have changed probably due to a change in composition. In fact, Raman spectrum for the sample that went under 700 °C NH_3 heat treatment at 0.5 mbar clearly shows that E^1_{2g} and A_{1g} MoS_2 Raman modes are completely vanished (see Figure S3 in Supplementary Information). Thus, we can affirm that there is no remaining MoS_2 nanosheets after the NH_3 heat treatments. We can also infer that there are no Mo atoms left on the top of the substrate, which means that Mo has desorbed in the form of a volatile compounds. However, XPS measurements performed on the treated samples confirm the presence of Mo in the Mo*3d* region (see below in Figure 8). Also, the 700°C temperature used for this experiment is lower than the formation temperature of MoO_3 gas. Moreover, there are no reports of the formation of volatile molecules in literature for the Mo-N binary system in this temperature range, which confirms the conversion of pristine MoS_2 into a MoN_x solid phase.

The rapid increase in R405 as soon as NH_3 valve is opened shows that the composition change is quasi-immediate at 50 mbar. In order to potentially control this modification, NH_3 heat treatments with a pressure lower than 50 mbar were performed. Figure 7 presents the R405 evolution starting at the 700 °C plateau under NH_3 for pressures between 0.5 and 50

mbar. The values of R405 on the Y-axis and of time on the X-axis have been normalized for better visualization.

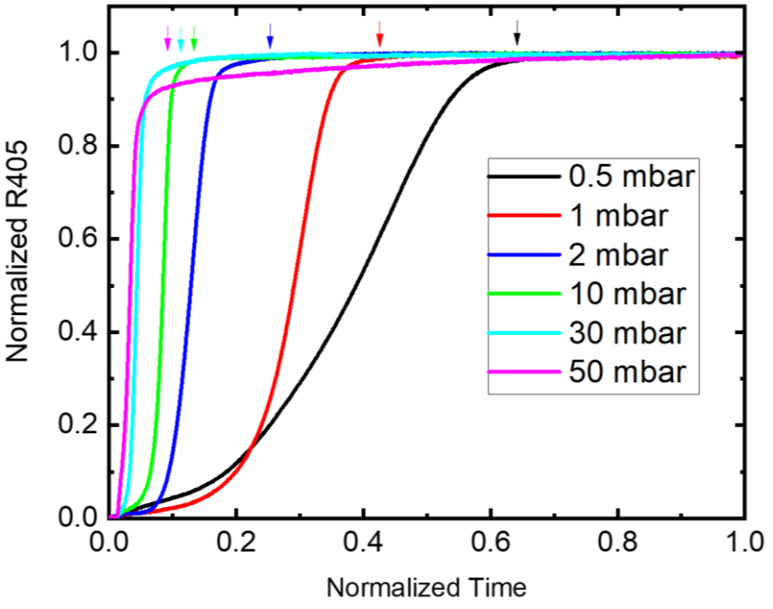

Figure 7: Evolution of the R405 component during the 700 °C NH_3 temperature plateau for different NH_3 pressures. For each curve, $\frac{dR405}{dt} \approx 0$ is represented by an arrow and is discussed in the next section.

We observe that the higher the NH_3 pressure, the faster the increase in R405 value and the quicker a plateau value is reached. This result indicates that the observed color change, and subsequently the composition and structural properties of the layer can be adjusted with the NH_3 pressure. Thus, the kinetics of the thermochemical conversion of MoS_2 is dependent on the NH_3 pressure. These aspects will be discussed in the next section.

To assess the changes in composition of MoS_2 at 700 °C under NH_3, we performed XPS measurements on the sample after the heat treatment. The Mo*3p*/N*1s* and Mo*3d* regions for the samples after 700 °C treatment under vacuum and under NH_3 with a regulated pressure of 0.5 mbar are represented in Figure 8 a) and b), respectively. In the Mo*3p*/N*1s* regions, we observe a clear difference between the samples treated at 700°C under vacuum and under NH_3 at 0.5 mbar. Indeed, a significant shoulder at around 398.0 eV appears after NH_3 treatment. Moreover, according to Table S1, we observe the respective appearance and disappearance of nitrogen and sulphur after the 700 °C NH_3 heat treatment. Considering the absence of significant evolution of the characteristic peaks of the other detected elements (oxygen, carbon and silicon) and the disappearance of S*2p* peak (peak not shown), nitrogen

cannot be bonded to any other element than molybdenum. Spectrum deconvolution indicates a peak at 397.9 eV which can be assigned to N*1s*. This N*1s* peak at 397.9 eV and the Mo$3p_{3/2}$ peak at 395.4 eV are close to the values reported by Cao et *al.*[23] (397.9 eV and 395.3 eV) suggesting that chemical bonds are formed between Mo and N.

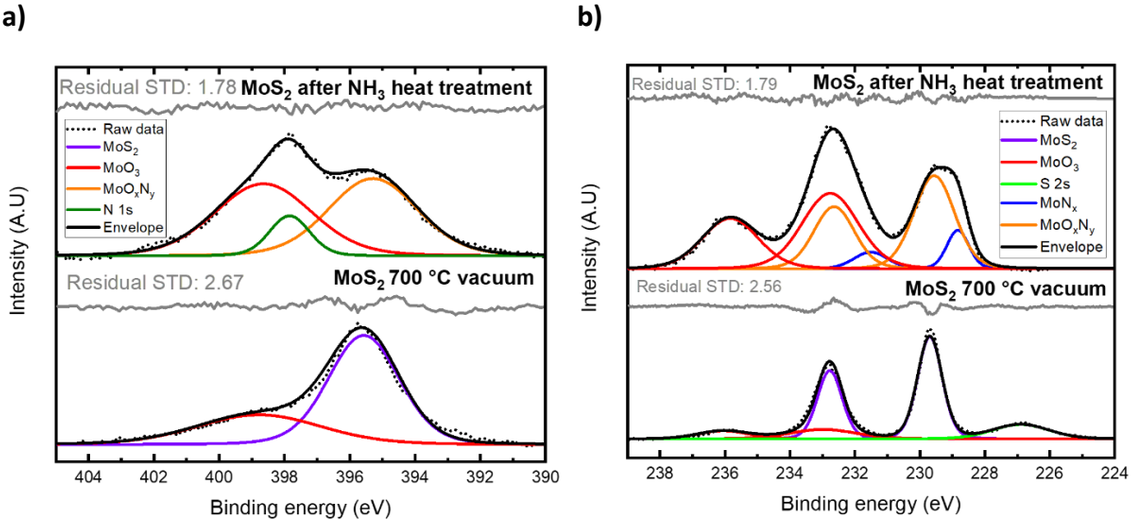

Figure 8: X-ray photoelectron spectra of a) Mo3p/N1s ; b) Mo3d of MoS_2 after 700 °C vacuum experiment and MoS_2 treated at 700 °C under NH_3 0.5 mbar.

In the Mo*3d* region, we observe a notable change in the XPS signal. First of all, after the NH_3 heat treatment, we can notice the absence of S*2s* signal (in agreement with the disappearance of the S*2p*), while Mo*3d* is still observed with multiple environments. This means that MoS_2 sample has been chemically converted during the NH_3 heat treatment. By deconvoluting Mo*3d* spectra, we can attribute the Mo$3d_{5/2}$ and Mo$3d_{3/2}$ peaks at 228.8 eV and 231.9 eV, respectively, to Mo-N bond [40,41]. But the main part of the spectra is composed of the Mo$3d_{5/2}$ and Mo$3d_{3/2}$ peaks at 229.5 eV and 232.6 eV. The Mo$3d_{5/2}$ binding energy is situated between those assigned to Mo^{4+} (230.0 eV) and Mo° (227.8 eV) [42]. Several studies attribute these peaks to the formation of Mo_2N [41,43–45]. Nevertheless, a significant increase in the atomic oxygen concentration is observed after the NH_3 heat treatment. Therefore, it is probably more accurate to attribute these peaks to a mixture of MoO_2 and Mo_2N [46]. The formation of this molybdenum oxynitride probably results from the exposition of the sample to air. Finally, the Mo$3d_{5/2}$ and Mo$3d_{3/2}$ peaks at 232.7 eV and 235.7 eV are assigned to a significant amount of MoO_3 (Mo^{6+}) also linked to air exposure after the heat treatment.

Journal of Vacuum Science & Technology A

IV. Discussion

Vacuum experiments at 700 °C do not show a chemical transformation of the MoS_2 film. In fact, only slight changes are observed on the *in situ* reflectance measurements during the heat treatment, caused by the potential degradation of the MoS_2 layer. This observation has been confirmed by Raman analysis where MoS_2 signal is preserved, which proves the conservation of MoS_2 crystallized nanosheets. Under NH_3 atmosphere, changes on the *in situ* reflectance measurements are observed suggesting the chemical conversion of MoS_2. By adjusting the NH_3 pressure during the heat treatment, it is possible to control the kinetics of the thermochemical reaction of MoS_2. Also, Raman analysis indicates that E^1_{2g} and A_{1g} MoS_2 Raman modes are completely vanished after NH_3 exposure. Finally, the XPS results reveal the conversion of Mo and the absence of S indicating the chemical conversion of MoS_2. The deconvolution of Mo*3d* and Mo*3p* spectra highlights the presence of Mo-N bond and confirms the chemical conversion of MoS_2 into MoN_x. From a thermodynamical point of view of the Mo-N system, this conversion is unexpected, except at high NH_3 pressure as the nitride compounds Mo_2N and MoN are characterized by a poor stability at normal conditions [47]. Therefore, we believe that the obtaining of MoN is related to kinetic issues, due to the high reactivity of NH_3. In fact, Marchand et *al.* [48–50] group were pioneers in the synthesis of molybdenum nitride from MoS_2 by reduction of sulphides by ammonia reactive heat treatments. Later, Ganin et *al.* [51] used the same method to prepare molybdenum nitrides and finally, Sun et a*l.* [13] and Cao et *al.* [23] have demonstrated the transformation of MoS_2 nanosheets exfoliated from bulk material into molybdenum nitride with ammonia and urea reactive heat treatments, respectively. As demonstrated in this work, the conversion of MoS_2 into MoN_x is experimentally possible but seems to lead to unstable phases which could explained the differences observed with thermodynamic investigations.

Finally, *in situ* reflectance results in function of the NH_3 pressures are used to have a better understanding of the kinetics of the involved reactions. For each NH_3 pressure, R405 values presented in Figure 7 are derivated in order to determine the points where $\frac{dR405}{dt} \approx 0$ corresponding to the moment where the MoS_2 conversion into MoN_x is completed. As in Tsakonas et *al.*[52] study, the reflectance reaches a plateau when no more chemical or morphological changes beyond the steady-state thermal dynamics are occurring. These points are represented by arrows on Figure 7. We extracted the values where $\frac{dR405}{dt} \approx 0$ and plotted

the evolution of the normalized time to complete the conversion with the NH_3 pressure in Figure 9. Then, a Van't Hoff's model has been applied using the following equation:

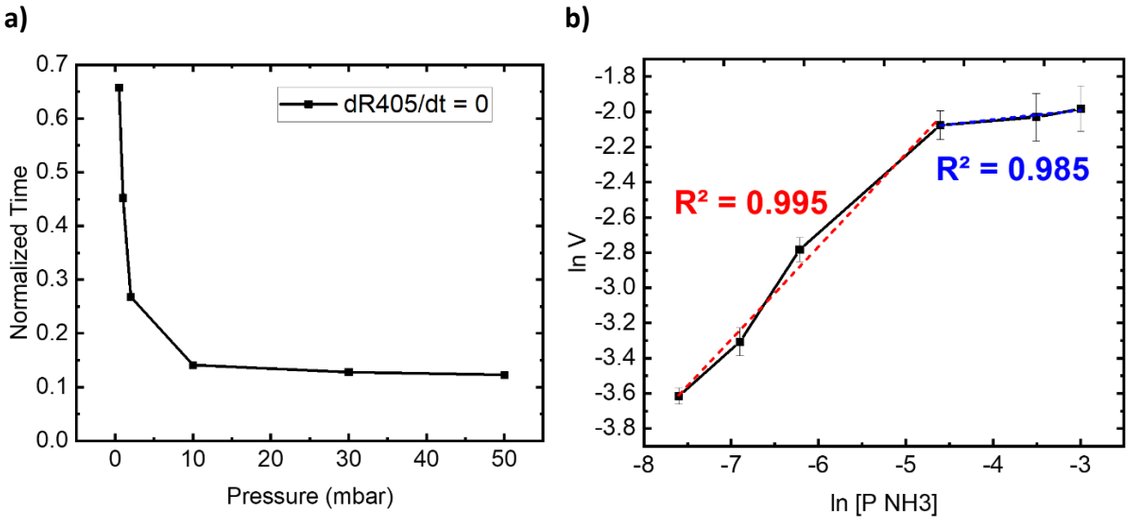

Figure 9: a) $\frac{dR405}{dt} \approx 0$ *for the different* NH_3 *pressures investigated ; b) application of the Van't Hoff's law.*

$$V = k.[MoS_2]^{\alpha}.[NH_3]^{\beta}$$

Where V is the overall rate of the reaction, k is a kinetic constant, $[MoS_2]$ and $[NH_3]$ are molar concentrations and α and β are the stoichiometric coefficients relative to the MoS_2 and NH_3, respectively. As shown in Figure 9 a), the conversion rate of MoS_2 into MoN_x is dependent on the NH_3 pressure which is directly related to NH_3 concentration $[NH_3]$. Thus, we can postulate that NH_3 is the limiting species and will impose the reaction rate. So, we can write:

$$V = k.[NH_3]^{\beta} \Leftrightarrow \ln(V) = \ln(k) + \beta\, ln[NH_3]$$

The curve $\ln(V) = f(ln[NH_3])$ is adjusted to fit the experimental points in Figure 9 b). Two different regimes seem to be distinguished. The first trend line indicates that the MoS_2 conversion into MoN_x depends linearly on the NH_3 pressure. This part corresponds to the heat treatment with a NH_3 pressure between 0.5 mbar and 10 mbar. It means that the kinetic limiting factor is the amount of NH_3 species at the MoS_2 surface leading to its conversion. The second trend line is constant suggesting that the MoS_2 conversion into MoN_x is independent of NH_3 pressure above 10 mbar. It means that we have a rapid MoS_2 conversion and thus that the limiting factor is the amount of MoS_2. If we focus on the first trend line, we can extract $\ln(k) = 0.29 \pm 0.32$ and $\beta = 0.51 \pm 0.05$ being the y-intercept and the slope, respectively.

V. Conclusions

In this work, we demonstrate the total conversion of a MoS_2 thin film into MoN_x through an NH_3 reactive heat treatment at 700 °C. Raman spectroscopy coupled with X-Ray photoelectron spectrometry confirmed this thermochemical conversion. We succeeded to exploit the experimental results, especially, *in situ* reflectance measurements and by applying a Van't Hoff law's to model the MoS_2 consumption by NH_3. This model highlights that the kinetic conversion can be controlled by adjusting the NH_3 pressure. The proposed method coupled with *in situ* measurements pave the way to the preparation of molybdenum nitride with a direct control of the reaction rate. Moreover, as MoS_2 is a well-controlled and conformal thin film deposited by ALD its conversion can give access to MoN_x thin films with a precise thickness control and an excellent conformability for applications with complex, small-sized and high aspect ratio architectures [53] . The thickness of the obtained MoN_x film make its structural characterization difficult although this problem can be solved by studying thicker films. Finally, this approach could be extended to the synthesis of a wide range of metal carbides and nitrides (MXenes) with the possibility of controlling their structural properties depending on the reaction rate. It paves the way to the development of new synthesis routes of 2D materials with a wide range of applications.

Acknowledgments

A part of this work, carried out on the Platform for Nanocharacterization (PFNC), was supported by the "Recherche Technologique de Base" program of French National Research Agency (ANR). The authors would like to thank Roman Reboud and Vincent Tabouret for their support and participation in the development of the home-made furnace.

Data Availability

The data that supports the findings of this study are available within the article [and its supplementary material].

Author Declarations

The authors have no conflicts to disclose.

References

See supplementary material at [insert URL]

Journal of Vacuum Science & Technology A

[1] K.S. Novoselov, A.K. Geim, S.V. Morozov, D. Jiang, Y. Zhang, S.V. Dubonos, I.V. Grigorieva, and A.A. Firsov, Science **306**(5696), 666–669 (2004).
[2] A. Goff, P. Aukarasereenont, C.K. Nguyen, R. Grant, N. Syed, A. Zavabeti, A. Elbourne, and T. Daeneke, Dalton Trans. **50**(22), 7513–7526 (2021).
[3] H. Xie, Z. Li, L. Cheng, A.A. Haidry, J. Tao, Y. Xu, K. Xu, and J.Z. Ou, Science **25**(1), 103598 (2022).
[4] M. Chhowalla, Z. Liu, and H. Zhang, Chem. Soc. Rev. **44**(9), 2584–2586 (2015).
[5] S.A. Han, R. Bhatia, and S.-W. Kim, Nano Converg. **2**(1), 17 (2015).
[6] N.K. Chaudhari, H. Jin, B. Kim, D. San Baek, S.H. Joo, and K. Lee, J. Mater. Chem. A **5**(47), 24564–24579 (2017).
[7] S. Singh, G.N. Arka, S. Gupta, and S.B. Prasad, in (Jamshedpur, India, 2021), p. 040017.
[8] M. Khazaei, M. Arai, T. Sasaki, C.-Y. Chung, N.S. Venkataramanan, M. Estili, Y. Sakka, and Y. Kawazoe, Adv. Funct. Mater. **23**(17), 2185–2192 (2013).
[9] Y. Zhong, X. Xia, F. Shi, J. Zhan, J. Tu, and H.J. Fan, Adv. Sci. **3**(5), 1500286 (2016).
[10] X. Xiao, H. Yu, H. Jin, M. Wu, Y. Fang, J. Sun, Z. Hu, T. Li, J. Wu, L. Huang, Y. Gogotsi, and J. Zhou, ACS Nano **11**(2), 2180–2186 (2017).
[11] Y. Wang, and Y. Ding, J. Mater. Chem. C **6**(9), 2245–2251 (2018).
[12] X. Xiao, H. Wang, P. Urbankowski, and Y. Gogotsi, Chem. Soc. Rev. **47**(23), 8744–8765 (2018).
[13] G.-D. Sun, G.-H. Zhang, and K.-C. Chou, J. Am. Ceram. Soc. **101**(7), 2796–2808 (2018).
[14] Y.-H. Joo, D.K. Nandi, R. Ramesh, Y. Jang, J.-S. Bae, T. Cheon, and S.-H. Kim, J. Alloys Compd. **858**, 158314 (2021).
[15] P. Alén, M. Ritala, K. Arstila, J. Keinonen, and M. Leskelä, J. Electrochem. Soc. **152**(5), G361 (2005).
[16] T.H. Kim, D.K. Nandi, R. Ramesh, S.-M. Han, B. Shong, and S.-H. Kim, Chem. Mater. **31**(20), 8338–8350 (2019).
[17] E. R. Braitwaite, and J. Haber, (1994).
[18] D. Jariwala, V.K. Sangwan, L.J. Lauhon, T.J. Marks, and M.C. Hersam, ACS Nano **8**(2), 1102–1120 (2014).
[19] X. Li, and H. Zhu, J. Materiomics **1**(1), 33–44 (2015).
[20] S. Cadot, O. Renault, M. Frégnaux, D. Rouchon, E. Nolot, K. Szeto, C. Thieuleux, L. Veyre, H. Okuno, F. Martin, and E.A. Quadrelli, Nanoscale **9**(2), 538–546 (2017).
[21] R. Marchand, X. Gouin, F. Tessier, and Y. Laurent, MRS Proc. **368**, (1994).
[22] R. Marchand, X. Gouin, F. Tessier, and Y. Laurent, in *Chem. Transit. Met. Carbides Nitrides*, edited by S.T. Oyama (Springer Netherlands, Dordrecht, 1996), pp. 252–273.
[23] J. Cao, T. Li, H. Gao, Y. Lin, X. Wang, H. Wang, T. Palacios, and X. Ling, Sci. Adv. **6**(2), eaax8784 (2020).
[24] J.L. Verble, and T.J. Wieting, Phys. Rev. Lett. **25**(6), 362–365 (1970).
[25] T.J. Wieting, and J.L. Verble, Phys. Rev. B **3**(12), 4286–4292 (1971).
[26] X. Li, J. Li, K. Wang, X. Wang, S. Wang, X. Chu, M. Xu, X. Fang, Z. Wei, Y. Zhai, and B. Zou, Appl. Phys. Lett. **109**(24), 242101 (2016).
[27] C. Lee, H. Yan, L.E. Brus, T.F. Heinz, J. Hone, and S. Ryu, ACS Nano **4**(5), 2695–2700 (2010).
[28] H. Li, Q. Zhang, C.C.R. Yap, B.K. Tay, T.H.T. Edwin, A. Olivier, and D. Baillargeat, Adv. Funct. Mater. **22**(7), 1385–1390 (2012).
[29] X. Zhang, X.-F. Qiao, W. Shi, J.-B. Wu, D.-S. Jiang, and P.-H. Tan, Chem. Soc. Rev. **44**(9), 2757–2785 (2015).
[30] L. Liang, and V. Meunier, Nanoscale **6**(10), 5394 (2014).
[31] Y. Yan, F. Li, Y. Gong, M. Yao, X. Huang, X. Fu, B. Han, Q. Zhou, and T. Cui, J. Phys. Chem. C **120**(43), 24992–24998 (2016).
[32] L. Yang, X. Cui, J. Zhang, K. Wang, M. Shen, S. Zeng, S.A. Dayeh, L. Feng, and B. Xiang, Sci. Rep. **4**(1), 5649 (2015).
[33] A. McCreary, A. Berkdemir, J. Wang, M.A. Nguyen, A.L. Elías, N. Perea-López, K. Fujisawa, B. Kabius, V. Carozo, D.A. Cullen, T.E. Mallouk, J. Zhu, and M. Terrones, J. Mater. Res. **31**(7), 931–944 (2016).
[34] Tuschel, (2020).
[35] S. Mattila, J.A. Leiro, M. Heinonen, and T. Laiho, Surf. Sci. **600**(24), 5168–5175 (2006).

Journal of Vacuum Science & Technology A

[36] Z. Zeng, Z. Yin, X. Huang, H. Li, Q. He, G. Lu, F. Boey, and H. Zhang, Angew. Chem. Int. Ed. **50**(47), 11093–11097 (2011).
[37] B. Li, L. Jiang, X. Li, P. Ran, P. Zuo, A. Wang, L. Qu, Y. Zhao, Z. Cheng, and Y. Lu, Sci. Rep. **7**(1), 11182 (2017).
[38] J. Griffin, D.C. Watters, H. Yi, A. Iraqi, D. Lidzey, and A.R. Buckley, Adv. Energy Mater. **3**(7), 903–908 (2013).
[39] A. Syari'ati, S. Kumar, A. Zahid, A. Ali El Yumin, J. Ye, and P. Rudolf, "Chem. Commun. **55**(70), 10384–10387 (2019).
[40] J. Qian, S. Li, J. Pu, Z. Cai, H. Wang, Q. Cai, and P. Ju, Surf. Coat. Technol. **374**, 725–735 (2019).
[41] T. Bécue, J.-M. Manoli, C. Potvin, G. Djéga-Mariadassou, and M. Delamar, J. Phys. Chem. B **101**(33), 6429–6435 (1997).
[42] J.-G. Choi, D. Choi, and L.T. Thompson, Appl. Surf. Sci. **108**(1), 103–111 (1997).
[43] G.-T. Kim, T.-K. Park, H. Chung, Y.-T. Kim, M.-H. Kwon, and J.-G. Choi, Appl. Surf. Sci. **152**(1–2), 35–43 (1999).
[44] C. Shi, A.M. Zhu, X.F. Yang, and C.T. Au, Appl. Catal. Gen. **293**, 83–90 (2005).
[45] D. Mckay, J.S.J. Hargreaves, and R.F. Howe, Catal. Lett. **112**(1–2), 109–113 (2006).
[46] H. Wu, and K. Lian, ECS Trans. **58**(25), 67–75 (2014).
[47] H. Jehn, in *Mo Molybdenum*, edited by H. Katscher, W. Kurtz, and F. Schröder (Springer Berlin Heidelberg, Berlin, Heidelberg, 1989), pp. 1–66.
[48] R.J. Marchand, X. Gouin, F. Tessier, and Y. Laurent, MRS Proc. **368**, (1994).
[49] F. Tessier, R. Marchand, and Y. Laurent, J. Eur. Ceram. Soc. **17**(15–16), 1825–1829 (1997).
[50] R. Marchand, F. Tessier, and F.J. DiSalvo, J. Mater. Chem. **9**(1), 297–304 (1999).
[51] A.Yu. Ganin, L. Kienle, and G.V. Vajenine, J. Solid State Chem. **179**(8), 2339–2348 (2006).
[52] C. Tsakonas, A.C. Manikas, M. Andersen, M. Dimitropoulos, K. Reuter, and C. Galiotis, Chem. Eng. J. **421**, 129434 (2021).
[53] Y. Jang, J.B. Kim, T.E. Hong, S.J. Yeo, S. Lee, E.A. Jung, B.K. Park, T.-M. Chung, C.G. Kim, D.-J. Lee, H.-B.-R. Lee, and S.-H. Kim, J. Alloys Compd. **663**, 651–658 (2016).

Journal of Vacuum Science & Technology A

a)

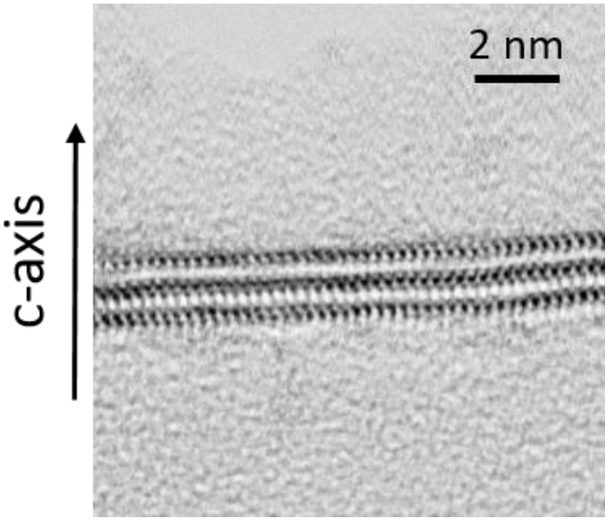

b)

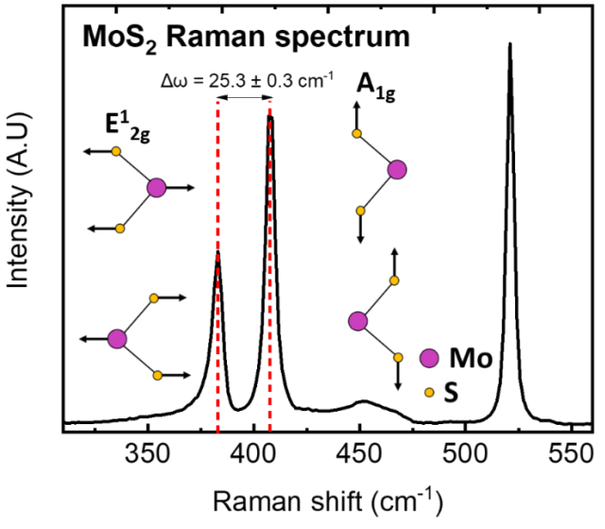

Journal of Vacuum Science & Technology A

PLEASE CITE THIS ARTICLE AS DOI: 10.1116/6.0002678

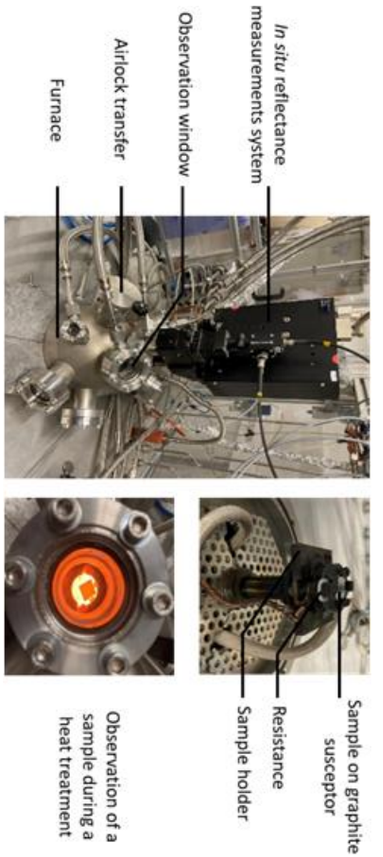

Journal of Vacuum Science & Technology A

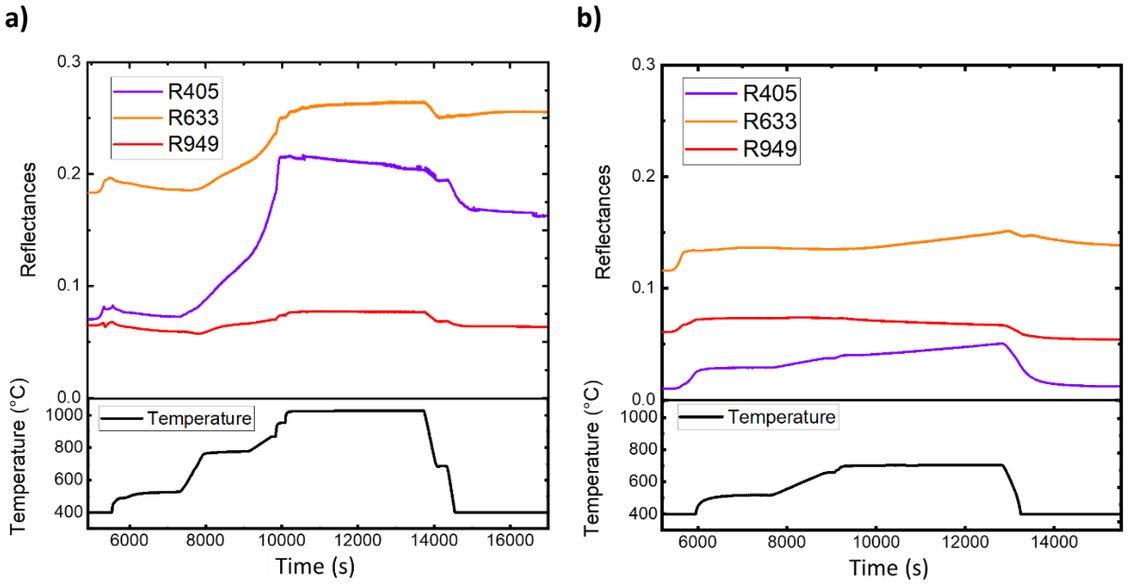

Journal of Vacuum Science & Technology A

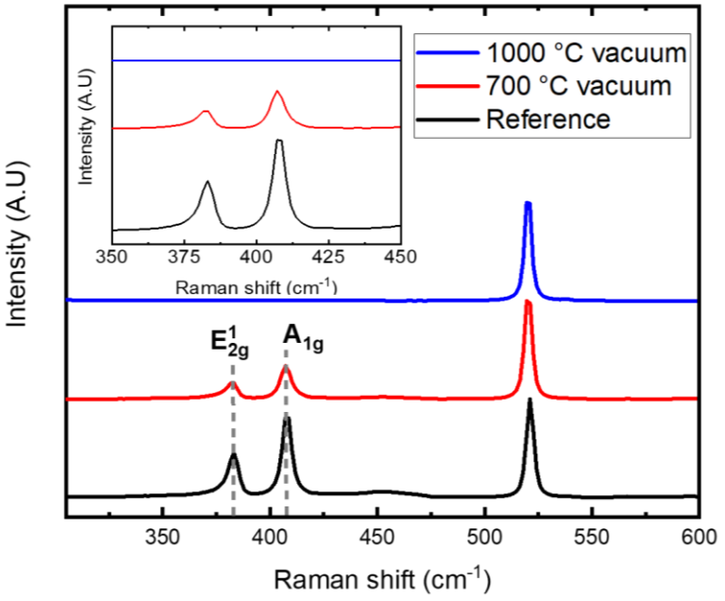

Journal of Vacuum Science & Technology A

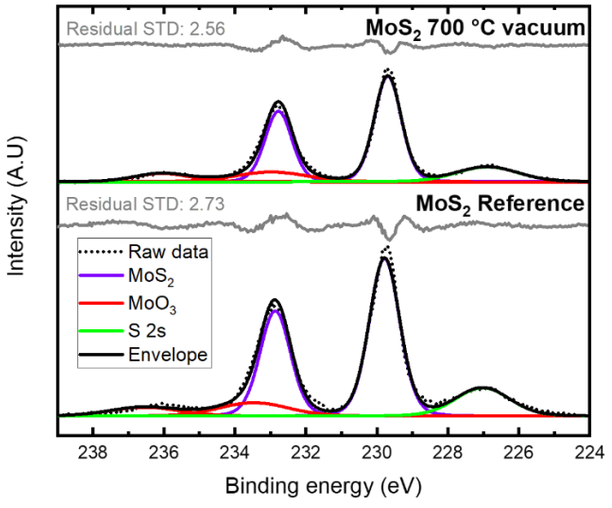

Journal of Vacuum Science & Technology A

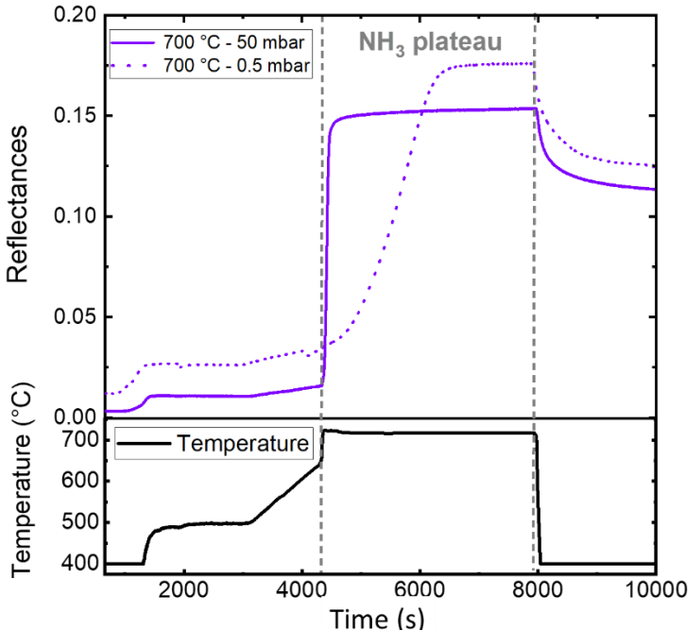

Journal of Vacuum Science & Technology A

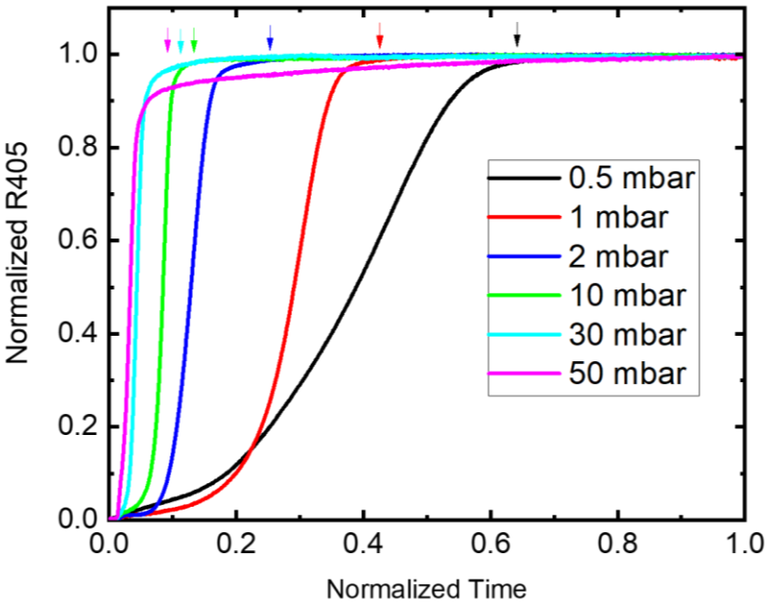

Journal of Vacuum Science & Technology A

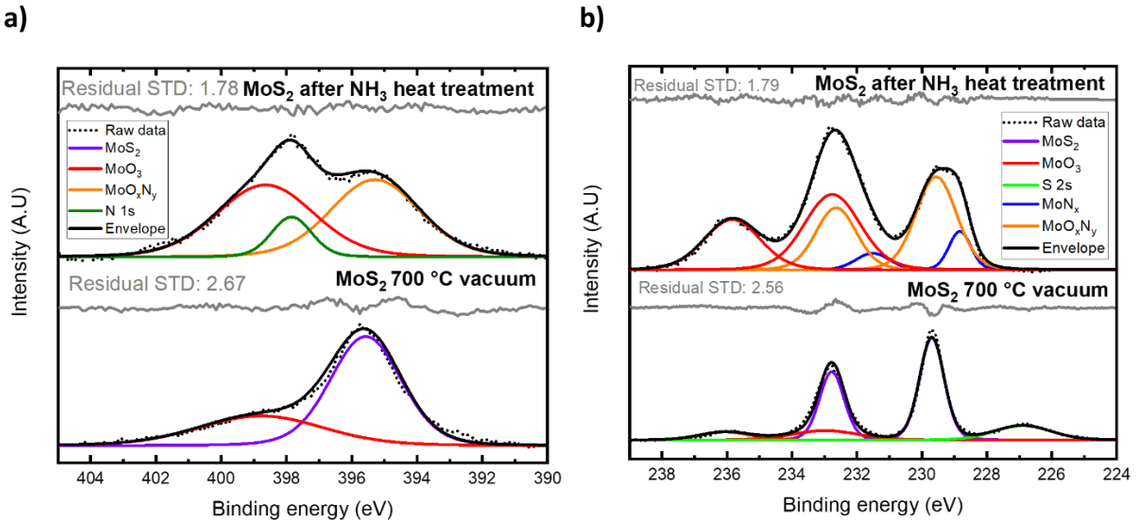

Journal of Vacuum Science & Technology A